Simulation of Heat Storage and Heat Regeneration in Phase Change Material

Khalid Ahmed Joudi , Ahmed Kasim Taha
Mechanical Engineering Department, College of Engineering, University of Baghdad

Abstract

The present study explores numerically the energy storage and energy regeneration during Melting and Solidification processes in Phase Change Materials (PCM) used in Latent Heat Thermal Energy Storage (LHTES) systems. Transient two-dimensional (2-D) conduction heat transfer equations with phase change have been solved utilizing the Explicit Finite Difference Method (FDM) and Grid Generation technique. A Fortran computer program was built to solve the problem. The study included four different Paraffin's. The effects of container geometrical shape, which included cylindrical and square sections of the same volume and heat transfer area, the container volume or mass of PCM, variation of mass flow rate of heat transfer fluid (HTF), and temperatures difference between PCM and HTF were all investigated.
Results showed that the PCMs in a cylindrical container melt and solidify quicker than the square container. The increase in mass flow rate and/or temperature difference decreases the time required for complete phase change. Paraffin's solidify quicker than they melt and store more energy than they release.

Keywords: Phase change material; Latent heat thermal energy storage; Melting; Solidification; Energy storage; Energy regeneration; Grid generation

الخلاصة:

تتحرى الدراسة الحالية عددياً الطاقة المخزونة والطاقة المتحررة أثناء عمليتي الذوبان والانجماد في مادة متغيرة الطور تستخدم في منظومات خزن الحرارة الكامنة. حلت معادلة انتقال الحرارة الانتقالية باتجاهين باستخدام طريقة الفروق المحددة الصريحة وبتقنية التوليد الشبكي. تم بناء برنامج حاسوبي بلغة فورتران لحل المسألة. تتضمن الدراسة أربعة برافينات متغيرة الطور، تأثير الشكل الهندسي لوحدة الخزن الذي تضمن المقطعين الدائري والمربع للحجم نفسه و مساحة انتقال الحرارة نفسها، حجم الخزان أو كتلة المادة المتغيرة الطور، تغيير نسبة التدفق لسائل نقل الحرارة، وفرق درجات الحرارة بين المادة متغيرة الطور وسائل نقل الحرارة.
بينت النتائج إن المادة متغيرة الطور في وحدات الخزن الحراري الاسطوانية تذوب وتتجمد أسرع مما في وحدات الخزن الحراري المربعة. زيادة نسبة التدفق و فرق درجات الحرارة يقلل الزمن اللازم لتغير الطور التام. البرافينات تتجمد أسرع مما تذوب وتخزن طاقة أكثر مما تحرر.

1. Introduction:

Thermal Energy Storage (TES) is essential to overcome the mismatches between the supply and consumption of energy or primary energy source variation, such as periodic variations of solar energy.

Phase Change Material (PCM) used for Latent Heat Storage (LHS) has received considerable attention attributed to its high storage density and isothermal nature of heat storage and release. There are many type of PCMs; organic, inorganic and their mixture that melt and solidify at a wide range of temperatures. This makes them attractive in a number of applications, such as; space and water heating, waste heat utilization, cooling and air-conditioning, and thermal control applications (Regin et al. 2008).

Paraffins have been used extensively as a latent heat energy material due to their advantages of a sufficiently high latent heat capacity, small volume changes during phase change, no sub-cooling effects, self-nucleating behavior, chemically stable, long freeze–melt cycle, nonpoisonous, noncorrosive, as well being available at low cost (Sharma et al. 2009).

Phase change is a transient, non-linear heat transfer mechanism with a moving solid-liquid interface, generally referred to as the "Moving Boundary " or "Stefan's" Problem(Lane 1983). The most common methods used for solving phase change problems are the enthalpy method and the effective heat capacity method (Lamberg et al. 2004). Phase change problems are usually solved with finite difference or finite element methods in accordance with the numerical approach. Previous studies can be divided into two main group; material research and heat exchanger development (Regin et al. 2008). PCMs with organic nature, inorganic and their mixture for heating and cooling applications has been investigated by many researchers. These applications can be divided into two main groups: thermal protection or inertia, and storage. PCMs store one hundred times more heat per unit mass than sensible storage materials such as water, or rock. Sarı and Karaipekli 2008 illustrated the basic types of PCM employed in LHTES systems and the main characteristics required for them. Hasan 1994 developed a simple tube-in-tube heat exchanger for TES with stearic acid as a PCM. He found that the melting front moves in the radial direction inward as well as in the axial direction from the top toward the bottom of the PCM tube. Phase transition was faster in a horizontal position rather than a vertical one. Esen et al. 1998 Considered two different shell and tube configurations where the PCM is packed in the tube and the HTF flows parallel to it in the shell and vice versa. It was concluded that the latent heat storage tank where the PCM is packed in the shell while the HTF flows through the tube stores much more solar energy in a given time as compared to the other configuration. Yimer 1996 developed a numerical model to determine the transient temperature distribution, solid/liquid interface location, and energy-storage capacity of a semi-transparent phase-change medium bounded between two concentric cylinders. Internal energy transfer occurs simultaneously by conduction and thermal radiation. Gong and Mujumdar 1998 have simulated the melting of a pure PCM in a rectangular container heated from below using the FEM. They obtained several complex and time-dependant flow patterns. Zivkovic and Fujii 2001 concluded that the rectangular container requires half of the melting time as for the cylindrical container of the same volume, using a simple computational model based on an enthalpy formulation. They also concluded that conduction within the

PCM in the direction of HTF flow, thermal resistance of the container's wall, and the effects of natural convection within the melt can be ignored for the conditions

investigated. Trp et al. 2006 studied the influence of the HTF inlet velocity and HTF inlet temperature as well as the influence of the tube length and outer tube radius on the total energy stored and recovered in shell and tubes LHTES system. Vyshak and Jilani 2007 made a comparative study of the total melting time of PCM packed in containers having three different geometric configurations, viz. rectangular, cylindrical and a cylindrical shell of the same volume and surface area of heat transfer. They employed a slightly modified enthalpy method, which enabled decoupling of the temperature and liquid fraction fields.

Mathematical Modeling:
2.1 Problem Description:

The present study involved two concentric tubes for the LHTES systems. The PCM fills the annular space between the two tubes, the HTF flows through the inner tube, and the outer tube is completely insulated.

During the charging process the PCM acts as a heat sink which receives energy from HTF whose temperature is higher than the PCM's melting temperature. The PCM melts and energy is stored as latent heat. During the discharging process, the PCM acts as a heat source to the HTF whose temperature is lower than the PCM's solidification temperature. The PCM solidifies and heat is released to the HTF.

Two geometrical configurations of the PCM's container were involved. The first was of a circular cross section and the second was of a square cross section, as shown in **Fig.1**. Three container volumes, i.e. mass of PCM were considered. The inner tube diameter (D_i) is 0.5 inch for all studied cases. For the

cylindrical configuration, the outer tube diameters (D_o) were 1, 1.5, and 2 inches that equal to 25.4, 38.1, and 50.8 mm respectively. The square configuration have the same volume so the side width (2w) were 22.51, 33.76, and 45.02 mm

respectively. Due to symmetry of the system, the computational domain is composed of only one quarter of the cross section.

Four types of paraffins having different melting points, of 28, 48, 64, and 84°C, suitable for solar applications, were employed as PCM, and water as HTF.

The study included the effect of different mass flow rates of the HTF at 1 and 3 l/min, and the effect of temperature difference between the PCM and the HTF at 15 and 25 °C.

2.2 Assumptions:

The following assumptions were made to simplify the phase change problem:
1. The PCM in each phase is homogeneous and isotropic.
2. The thermo-physical properties of the PCM are independent of temperature, but they are different form phase to phase.
3. The effect of natural convection in the liquid phase of PCM is not taken into account.
4. No internal heat generation , and all radiation effects are neglected.
5. The tube wall is very thin so that its thermal resistance can be neglected.

2.3 Governing Equations:

The energy equation for transient two dimensional (2-D) conduction heat transfer with phase change can be written as;

$$\rho_b c_b \frac{\partial T}{\partial t} = k_b \left[\frac{\partial^2 T}{\partial x^2} + \frac{\partial^2 T}{\partial y^2} \right]$$

The subscripts b denote the material properties for each phase. The physical fact that the phase change takes place in a temperature interval (from T_1 to T_2) can be used. Thus;
$b = s$ (solid phase properties) when $T < T_1$
$b = m$ (mushy zone properties) when $T_1 \leq T \leq T_2$

b = l   (liquid phase properties)
when $T > T_2$
The density and the thermal conductivity of the mushy zone can be estimated as an arithmetic average;

$$\rho_m = \frac{1}{2}(\rho_s + \rho_l) , \quad k_m = \frac{1}{2}(k_s + k_l)$$

While the specific heat can be found from the effective heat capacity method (Lamberg et al.2004);

$$c_m = c_{eff} = \frac{LH}{T_2 - T_1} + \frac{1}{2}(c_{ps} + c_{pl})$$ (4)

3. Numerical Solution:
3.1 Body-Fitted Coordinate System:

The nature of numerical calculations of the zone requires a proper treatment of the boundary conditions. The system which is made to generate a grid, might bring about a slow numeric convergence. This has encouraged the search for other methods to generate grids. One method includes the generation of curvilinear coordinate systems with coordinate lines coincident with all boundaries of the physical domain. This is called a body fitted coordinate (BFC) system. Regardless of the shape of the body in the physical plane, all the numerical computations are achieved in the form of a rectangular grid in the computational domain, as shown in **Fig.**

3.2 Grid Generation:

The method for generation of a curvilinear body fitted coordinate system is based on solution of a set of elliptic partial differential equations. The most common elliptic partial differential equations used for grid generation in two-dimensions is the Laplace equation in the form, (Hoffmann 1998);

$$\frac{\partial^2 \zeta}{\partial x^2} + \frac{\partial^2 \zeta}{\partial y^2} = 0$$ (5)

$$\frac{\partial^2 \eta}{\partial x^2} + \frac{\partial^2 \eta}{\partial y^2} = 0$$ (6)

However, computations must take place in a rectangular domain with uniform grid spacing. To transform the elliptic PDEs, the dependent and independent variables are interchanged and these equations become;

$$\alpha \frac{\partial^2 x}{\partial \zeta^2} - 2\beta \frac{\partial^2 x}{\partial \zeta \partial \eta} + \gamma \frac{\partial^2 x}{\partial \eta^2} = 0$$ (7)

$$\alpha \frac{\partial^2 y}{\partial \zeta^2} - 2\beta \frac{\partial^2 y}{\partial \zeta \partial \eta} + \gamma \frac{\partial^2 y}{\partial \eta^2} = 0$$ (8)

The system of elliptic Equations (7) and (8) will be solved by the Successive Over-Relaxation (S. O. R.) method in the computational domain (ζ, η) in order to provide the grid point locations in the physical space (x, y) as follows, (Petrovic and Stupar 1996);

$$x_{(i, j)} = (1-RF)\, x^o_{(i, j)} + [(\alpha_{(i, j)}/\Delta\zeta^2)(x_{(i+1, j)} + x_{(i-1, j)}) - (\beta_{(i, j)}/2\Delta\zeta.\Delta\eta)\,(x_{(i+1, j+1)} - x_{(i+1, j-1)} - x_{(i-1, j+1)} + x_{(i-1, j-1)}) + (\gamma_{(i, j)}/\Delta\zeta^2)(x_{(i, j+1)} - x_{(i, j-1)})]\,RF$$ (9)

$$y_{(i, j)} = (1-RF)\, y^o_{(i, j)} + [(\alpha_{(i, j)}/\Delta\zeta^2)(y_{(i+1, j)} + y_{(i-1, j)}) - (\beta_{(i, j)}/2\Delta\zeta.\Delta\eta)\,(y_{(i+1, j+1)} - y_{(i+1, j-1)} - y_{(i-1, j+1)} + y_{(i-1, j-1)}) + (\gamma_{(i, j)}/\Delta\zeta^2)(y_{(i, j+1)} - y_{(i, j-1)})]\,RF$$ (10)

1057

3.3 Explicit Finite Difference Method:

The explicit finite difference method includes the calculation of the temperature for a next time $(t + \Delta t)$ in terms of the temperature at the previous time (t) for the node (i, j) and to its neighboring nodes. In each node in the grid, the temperature will be known at time $(t = 0)$ from the initial condition of the problem. So, the temperature for each node will be obtained at the new time step by marching forward in time. It is possible, by the use of time steps Δt to arrive at the steady state and obtain the distribution of temperature, (Anderson 1995).

the governing equation (1), may be transformed from Cartesian coordinates into general coordinates as follows;

$$\frac{\partial T}{\partial t} = \frac{k_b}{\rho_b c_{pb}} [(\lambda \frac{\partial T}{\partial \zeta} + \sigma \frac{\partial T}{\partial \eta} + \alpha \frac{\partial^2 T}{\partial \zeta^2} - 2\beta \cdot \frac{\partial^2 T}{\partial \zeta \partial \eta} + \gamma \frac{\partial^2 T}{\partial \eta^2})/J^2] \qquad (11)$$

Transformation of the time derivative of temperature, using forward differences, at node (i, j), through the periodic from (t) to time $(t + \Delta t)$ takes the following forms;

$$\frac{\partial T}{\partial t} = \frac{T_{(i,j)}^{n+1} - T_{(i,j)}^{n}}{\Delta t} \qquad (12)$$

Where:

Represents the temperature at $(t + at)$.

Represents the temperature at (t).

$$\frac{\partial T}{\partial \zeta} = \frac{T_{(i+1,j)} - T_{(i-1,j)}}{2\Delta \zeta} \qquad (13)$$

And, the central differences will be used to transform the diffusion terms, as follows;

$$\frac{\partial^2 T}{\partial \zeta^2} = \frac{T_{(i+1,j)} - 2T_{(i,j)} + T_{(i-1,j)}}{\Delta \zeta^2} \qquad (14)$$

$$\frac{\partial T}{\partial \eta} = \frac{T_{(i,j+1)} - T_{(i,j-1)}}{2\Delta \eta} \qquad (15)$$

$$\frac{\partial^2 T}{\partial \eta^2} = \frac{T_{(i,j+1)} - 2T_{(i,j)} + T_{(i,j-1)}}{\Delta \eta^2} \qquad (16)$$

$$\frac{\partial^2 T}{\partial \zeta \partial \eta} = \frac{T_{(i+1,j+1)} - T_{(i+1,j-1)} - T_{(i-1,j+1)} + T_{(i-1,j-1)}}{4\Delta \zeta \cdot \Delta \eta} \qquad (17)$$

Now, the energy equation (11) will be transformed into a system of linear equations, as follows;

$$T_{(i,j)}^{n+1} = T_{(i,j)}^{n} + \Delta t [\alpha_b ((\lambda_{(i,j)} \frac{T_{(i+1,j)}^{n} - T_{(i-1,j)}^{n}}{2\Delta \zeta} + \sigma_{(i,j)} \frac{T_{(i,j+1)}^{n} - T_{(i,j-1)}^{n}}{2\Delta \eta}$$
$$+ \alpha_{(i,j)} \frac{T_{(i+1,j)}^{n} - 2T_{(i,j)}^{n} + T_{(i-1,j)}^{n}}{\Delta \zeta^2}$$
$$- 2\beta_{(i,j)} \frac{T_{(i+1,j+1)}^{n} - T_{(i+1,j-1)}^{n} - T_{(i-1,j+1)}^{n} + T_{(i-1,j-1)}^{n}}{4\Delta \zeta \cdot \Delta \eta}$$
$$+ \gamma_{(i,j)} \frac{T_{(i,j+1)}^{n} - 2T_{(i,j)}^{n} + T_{(i,j-1)}^{n}}{\Delta \eta^2})/J^2)] \qquad (18)$$

3.4 Solution Procedure:

A computer program in FORTRAN 90 language was built to solve the phase change problem. At first, the constants and variables were defined which included the thermo-physical properties of the PCM, the initial and boundary conditions, the dimensions of the geometry, number of nodes and the maximum time step (Δt_{max}) that ensures the stability of the solution. The computer program consists of two main parts, the first part is the grid generation. This part starts from the information of the geometry and then the 2D grids consist of many subroutines for transforming the physical plane (x, y) to the

computational plane (ζ, η) in a Body-Fitted coordinate system. The second part is the solution of the governing equations. This part starts from initial specifications of all fields of the dependent variables and the transformation parameters that were obtained from the grid generation. The final set of algebraic discretized equations is solved by the explicit finite difference method.

4. Results And Discussion:

4.1 Temperature Profile:

The temperature profiles are presented for a typical peripheral point at the container surface. This represents the last point affected by the heat source or sink and indicates complete melting or solidification time.

In general, the temperature profile can be divided into three main typical stages for melting and solidification as shown in **Fig. 3**. In the first stage; for melting, the temperature of the PCM increases linearly from its initial value till the lower limits of the melting range. While in solidification, the temperature of the PCM decreases linearly from its initial value till the upper limits of the solidification range.

In the second stage; the temperature of the PCM remains at a nearly constant value about the melting or solidification temperature. The temperature range varies from 1 to 3 $^{\circ}$C, which represent the lower and the upper limits of melting or solidification temperature range. The end of this stage means that the material is totally melted or solidified, i.e. the phase is completely changed.

In the third and last stage; the temperature of the PCM changes linearly again but at a lower rate due to a small temperature difference between the PCM and HTF than the first stage. In melting, the temperature rises to a temperature that equals the HTF temperature and then

remain constant. While in solidification, the temperature of the PCM decreases to a final temperature that equals the HTF temperature and then remains constant.

The temperature history for different paraffins have the same profile in all studied cases. **Fig. 4** shows the temperature history during melting process and **Fig. 5** shows the temperature history during solidification process for paraffin 48, which is chosen as a typical case. Paraffin 48 starts melting at 47 $^{\circ}$C and totally melts at 49 $^{\circ}$C, while it starts solidifying at 49 $^{\circ}$C and totally solidifies at 47 $^{\circ}$C.

These two figures show the effect of geometrical shape on the temperature profile. It is clear from the results that the PCM stored in the circular cross section container melts and solidifies quicker than that stored in square cross section container, and the PCM solidified quicker than it melts.

The results revealed that the greatest effect is related to the temperature difference as shown in **Fig. 6**. The temperature difference is the dominant factor on the heat transfer rates. Therefore, the effect of the mass flow rate of the HTF become insignificant at the higher temperature difference as shown in **Fig. 7**.

The effect of mass flow rate is translated as an effect of the convective heat transfer coefficient. **Fig. 8** and **Fig. 9** show the effect of the different convective heat transfer coefficients h_f on the temperature profile at 25 $^{\circ}$C and at 15 $^{\circ}$C temperature difference respectively. As mentioned before, one can note that the effect of the convective heat transfer coefficient becomes significant at the lower temperature difference value.

4.2 Temperature Distribution:

Fig.10 shows the temperature distribution during a melting process, and **Fig. 11** shows the temperature distribution during a

Solidification process at different time intervals. In all studied cases the circular cross section container melts and solidifies quicker than the square cross section container. In early time steps, the temperature distribution appears the same for both container shapes. Later, the square cross section container shows a higher resistance for melting or solidification at its corner due to the longer distance from the heat source or heat sink. Therefore, part of the PCM stays solid at the corner of the square cross section container during melting, while the whole PCM is melted in the circular cross section container. The same thing occurs in solidification where part of the PCM stays liquid at the corner of the square cross section container, while the PCM in the circular cross section container is totally solidified.

4.3 Time of melting and solidification:

Melting or Solidification time is defined as the time required to completely change the material from one phase to the other. Also, it is defined as the time required for charging or discharging energy. It is a very important factor in design and development of LHTES systems.

The effect of various factors on melting and solidification time are discussed in the following;

a. Effect of the Geometrical Design:
The results show that the PCM in a cylindrical container melts and solidifies quicker than in the rectangular container for the same volume (i.e. the same mass of the PCM) and same inner tube diameter (i.e. the same heat transfer area) for all studied cases as shown in **Fig. 4**, **5**, **10**, and **11**.

b. Effect of Container Volume:
As expected, the increase in container volume leads to increases in melting and solidification time as a result of the larger mass of the PCM and higher energy stored or regenerated. From **Fig. 12**, one can note that increasing of the cylindrical container diameter from 1 inch (i.e. aspect ratio 2) to

2 inches (i.e. aspect ratio 4) leads to increasing melting or solidification time from 5 to 10 times.

c. Effect of the PCM type:
Paraffin 48 has a good latent heat but low thermal conductivity. Therefore, it needs the longest time for melting and solidification. Paraffin 84 has the least latent heat but the highest thermal conductivity. Therefore, it melts and solidifies quicker than other three PCMs, as shown in **Fig. 12**.

d. Effect of initial and boundary conditions:
Fig. 13 shows that decreasing the temperature difference from 45°C to 35°C increases the melting time by 40 minutes. Whilst decreasing the temperature difference from 25°C to 15°C increases the melting time by 150 minutes. It is concluded that the reduction of the temperature difference has a more pronounced effect on melting and solidification time at lower values of ΔT.

Increasing the mass flow rate of the HTF leads to shorter melting and solidification times. **Fig. 14** shows this effect. Increasing mass flow rate from 1 to 2 l/min decreases the melting time by only 5 minutes. Therefore, the effect of the mass flow rate is less pronounced than the effect of the temperature difference. The effect of mass flow rate can be translated into the effect of convective heat transfer coefficient. This effect is much more evident at the lower value of temperature difference as shown in **Fig. 15**.

In all cases, the results show that the solidification time is shorter than the melting time. This means that the PCM needs more time to absorb energy than the time needed to release energy. The difference between melting and solidification times is related to the nature of the PCM and its thermo-physical properties. During solidification, liquid PCM freezes on the heat transfer surfaces and an immobile layer of solid material continuously grows as it gives up heat of

fusion. This solid layer, generally, has a higher thermal conductivity and heat transfer is improved, which in turn decreases the energy release time.

4.4 Energy Storages and Energy Regeneration:

The mass flow rate of the HTF, in the range investigated, has no significant effect on energy storage or regeneration. Its only effect is on the time of charging or discharging energy. Increasing the mass flow rate accelerates the period of melting and solidification. Increasing the temperature difference between HTF and PCM decreases the energy receival/retrieval time, as well as increasing the share of sensible heat of the total energy stored or regenerated.

The most important factor on the energy storage and energy regeneration is the thermo-physical properties of the PCM such as; latent heat, heat capacity, and density.

The present results show that the heat storage is higher than the heat generation as shown in **Fig. 16** and **Fig. 17**. The difference between energy stored and energy regenerated is related to the nature of the PCM and its thermo-physical properties. PCM receives energy initially as a solid phase during melting and stores energy in the liquid phase. The inverse occurs when energy is extracted from the liquid phase during solidification and some of energy may be reserved in the solid material.

5. Conclusions:

1. Temperature history have the same profile in all studied cases.
2. Temperature difference between the PCM and the HTF is the dominant factor on the heat transfer rates.
3. Mass flow rate of the HTF becomes insignificant at the higher temperature difference.

4. Cylindrical container melts/solidifies quicker than the square container.
5. Melting time is longer than solidification time.
6. Heat storage is higher than heat regeneration.

References:

- Anderson, D.J. (1995), "Computational Fluid Dynamics-The Basics with Applications", McGraw-Hill, NewYork.

- Esen, M. and Durmus, A., (1998), "Geometric design of solar-aided latent heat store depending on various parameters and phase change Materials", Solar Energy;62(1):19–28.

- Gong, Z.X. and Mujumdar, A.S., (1998), "Flow and Heat Transfer in Convection-Dominated Melting in a Rectangular Cavity Heated from below", Int. J. Heat Mass Transfer, Vol.14, pp.2573-2580.

- Hasan, A., (1994), "Thermal Energy Storage System with Stearic Acid as Phase Change Material", Energy Conversion and Management, 35, pp.843-856.

- Hoffmann, K. A. and Chiang, T. S. ,(1998), "Computational Fluid Dynamics", Engineering Education System, 3rd Ed.,Vol.I.

- Lamberg, P., Reijo Lehtiniemi, Anna-Maria Henell, (2004), "Numerical and experimental investigation of melting and freezing processes in phase change material storage", International Journal of Thermal Sciences 43, 277–287.

- Lane G., (1983): Solar Heat Storage: Latent Heat Material, vol. 1, CRC Press, Boca Raton, FL.

- Petrovic, Z. and Stupar, S. (1996), " Computational Fluid Dynamics, Part One", University of Belgrade,

- Mechanical Engineering Faculty, Belgrade.

- Regin A.F., Solanki S.C., and Saini J.S. (2008), "Heat transfer characteristics of thermal energy storage system using PCM capsules: A review ", Renewable and Sustainable Energy Reviews 12 2438–2458.

- Sari A., Karaipekli A., (2008), "Capric–myristic acid/expanded perlite composite as form-stable phase change material for latent heat thermal energy storage", Renewable Energy 33, 2599–2605.

- Sharma A., Tyagi V.V., Chen C.R., and Buddhi D., (2009), "Review on thermal energy storage with phase change materials and applications", Renewable and Sustainable Energy Reviews 13, 318–345.

- Trp, A., Kristian Lenic, Bernard Frankovic, (2006), "Analysis of the influence of operating conditions and geometric parameters on heat transfer in water-paraffin shell-and-tube latent thermal energy storage unit", Applied Thermal Engineering 26, 1830–1839.

- Vyshak, N.R. and Jilani, G., (2007), "Numerical analysis of latent heat thermal energy storage system", Energy Conversion and Management 48; 2161–2168.

- Yimer, B., (1996), "Thermal Radiation Effects in Phase-Change Energy Storage Systems", Energy Vol. 21, No. 12, pp. 1277-1286.

- Zivkovic, B. and Fujii, I., (2001), " An Analysis of Isothermal Phase Change of Phase Change Materials within rectangular and cylindrical containers", Solar Energy Vol. 70, No. 1, pp. 51–61
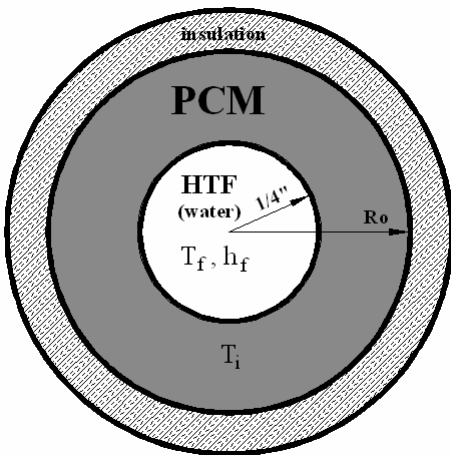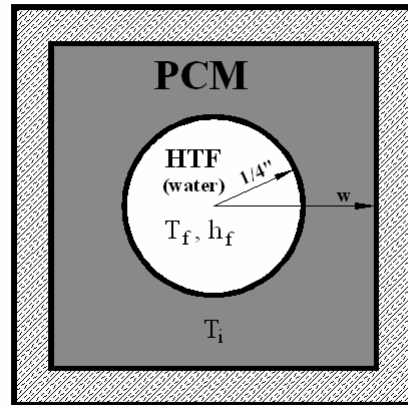
(a) cylindrical container   (b) Rectangular container

Figure 1 Two geometrical designs considered in the present study, same volume, same inner tube diameter.
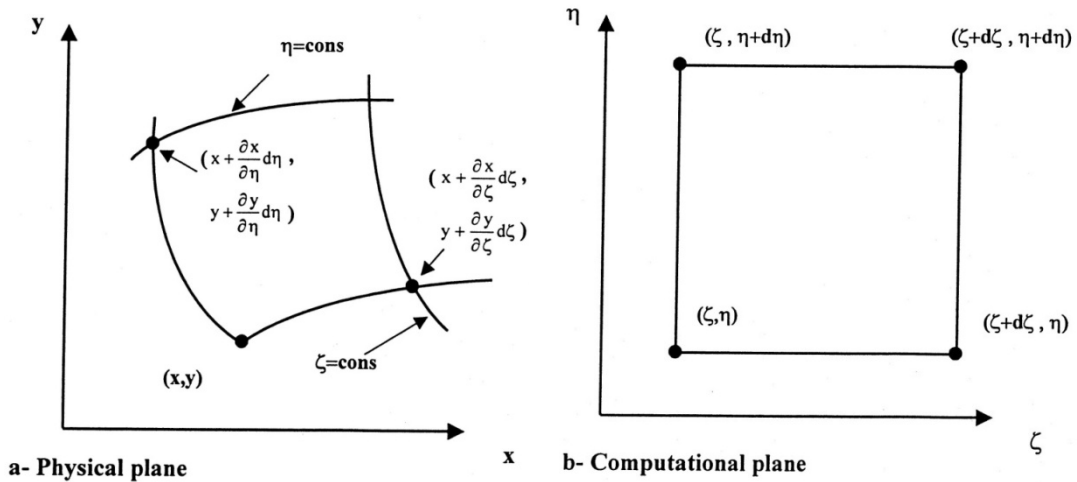
Figure 2 Element transformation from the physical to the computational plane.
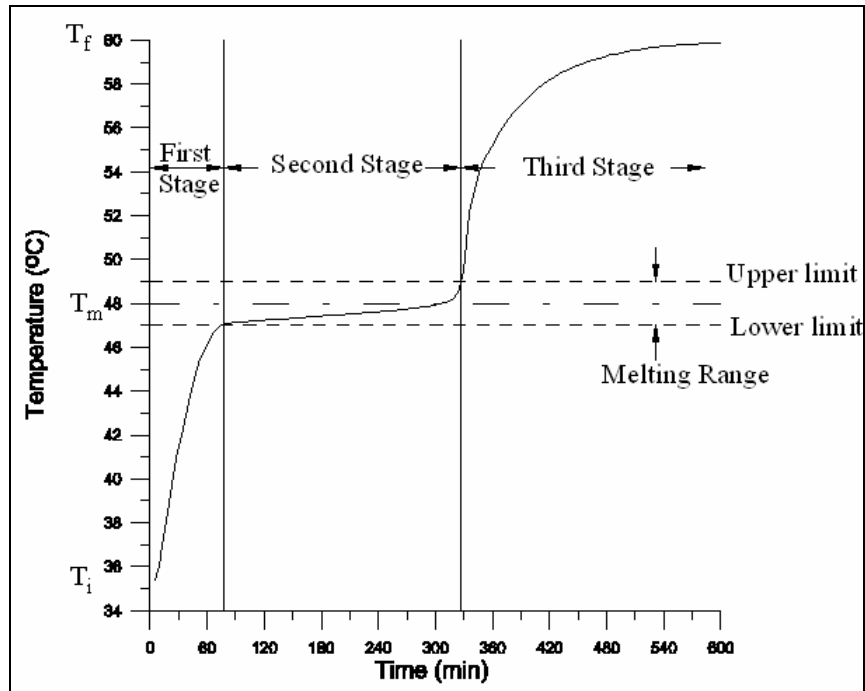
(a) Melting process
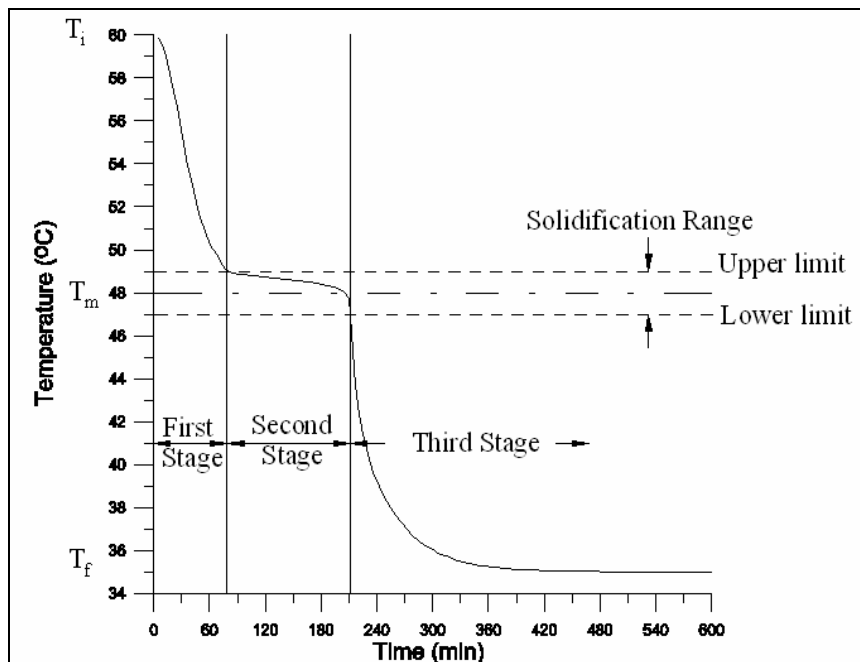
(b) Solidification process

Figure 3 Typical Temperature-Time profile for selected case. PCM2/Vol.3; $\Delta T=25^{o}C$, $m_f=3$ l/min
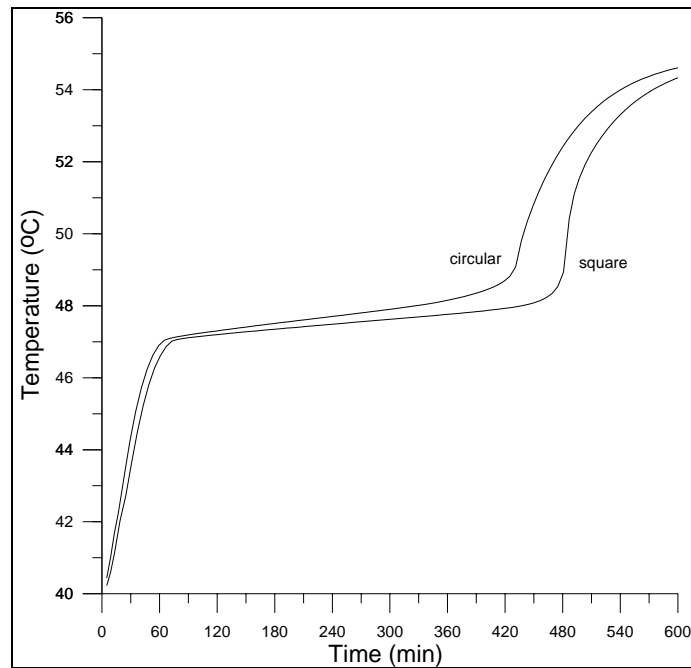
Figure 4 Temperature History during Melting Process for two geometrical designs (circular and square container). PCM2/Vol.3; $\Delta T = 15$ °C, $m_f = 3$ l/min
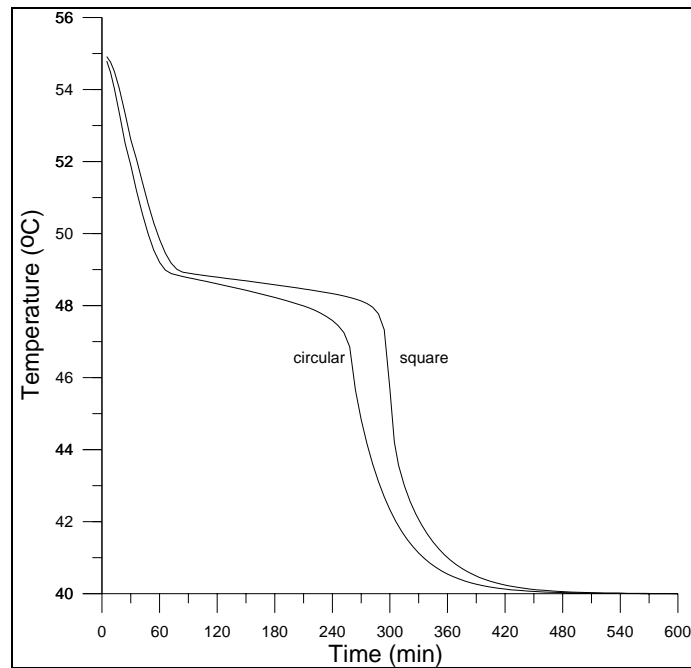
Figure 5 Temperature History during solidification Process for two geometrical designs (circular and square container). PCM2/Vol.3; $\Delta T = 15$ °C, $m_f = 3$ l/min.
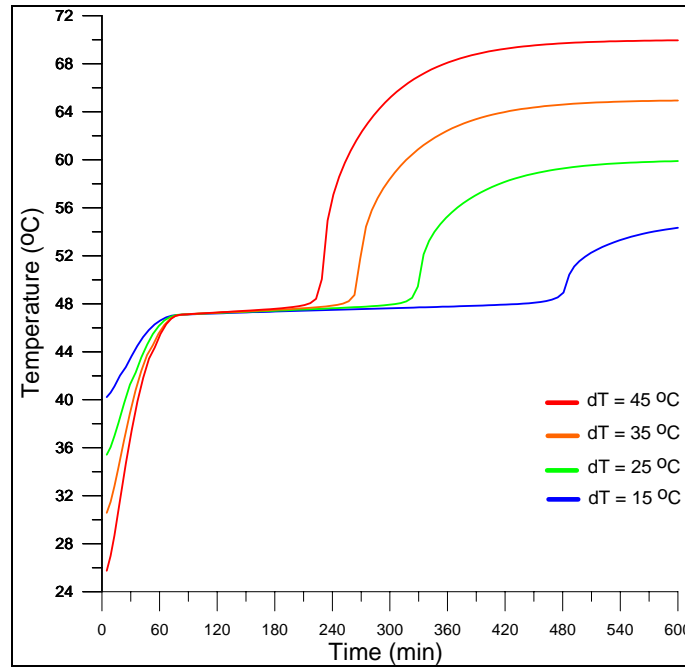
Figure 6 Temperature History during Melting Process of Paraffin (48 ^{o}C) at various Temperature difference (dT =T_f - T_i); 15, 25, 35 and 45 (^{o}C) ; m_f = 3 l/min
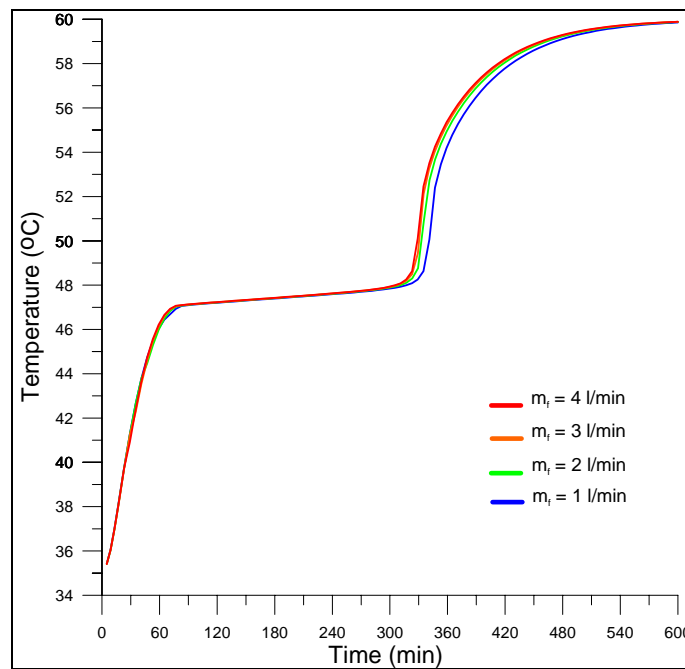
Figure 7 Temperature History during Melting Process of Paraffin (48 ^{o}C) at different mass flow rate; 1, 2, 3 and 4 (l/min), ΔT = 25 ^{o}C
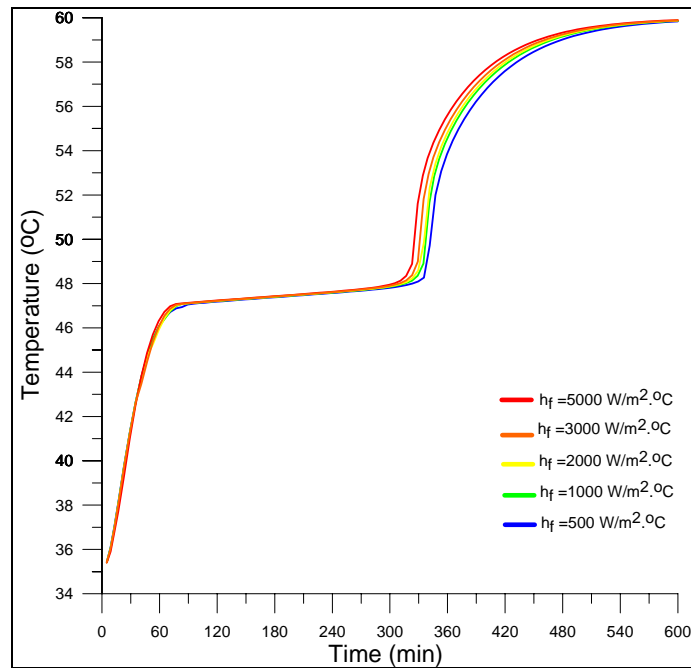
Figure 8 Temperature History during Melting Process of Paraffin (48 ^{o}C) at different Convection Heat Transfer Coefficient (h$_f$); 500, 1000, 2000, 3000 and 5000 (W/m^2.^{o}C), ΔT =(T$_f$ - T$_i$)=25 ^{o}C
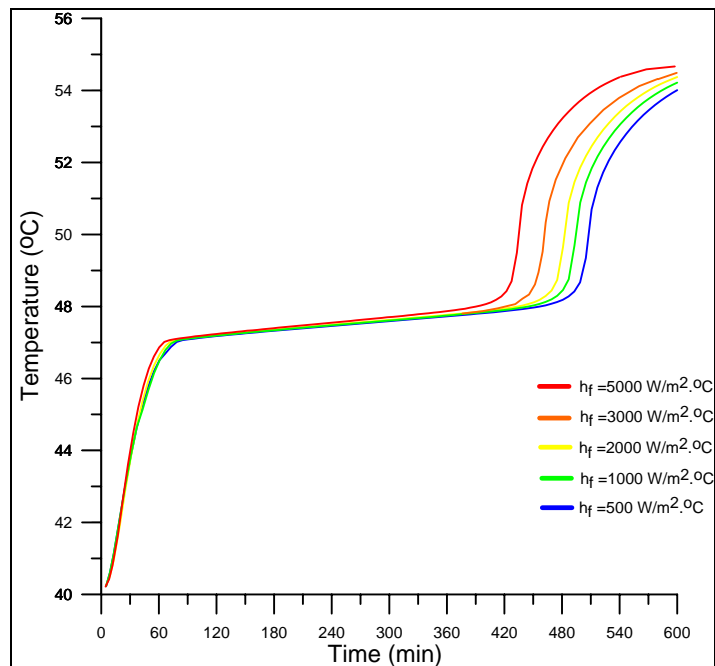
Figure 9 Temperature History during Melting Process of Paraffin (48 ^{o}C) at different Convection Heat Transfer Coefficient (h$_f$); 500, 1000, 2000, 3000 and 5000 (W/m^2.^{o}C), ΔT =(T$_f$ - T$_i$)=15 ^{o}C

After 1 hour   After 2 hour   After 3 hour
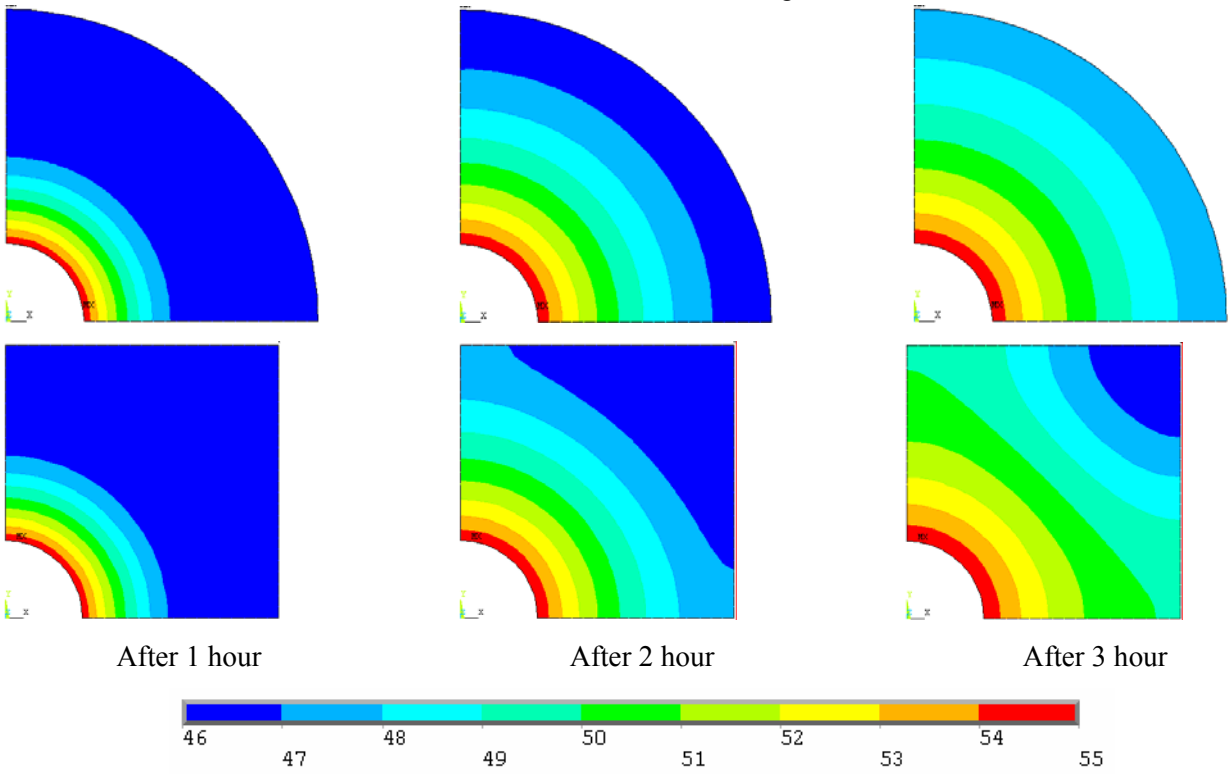
Figure 10 Temperature Distributions at Different Time during Melting Process.
PCM2/Vol.3; $\Delta T = 15$ ℃, $m_f = 1$ l/min.

After 1 hour   After 2 hour   After 3 hour
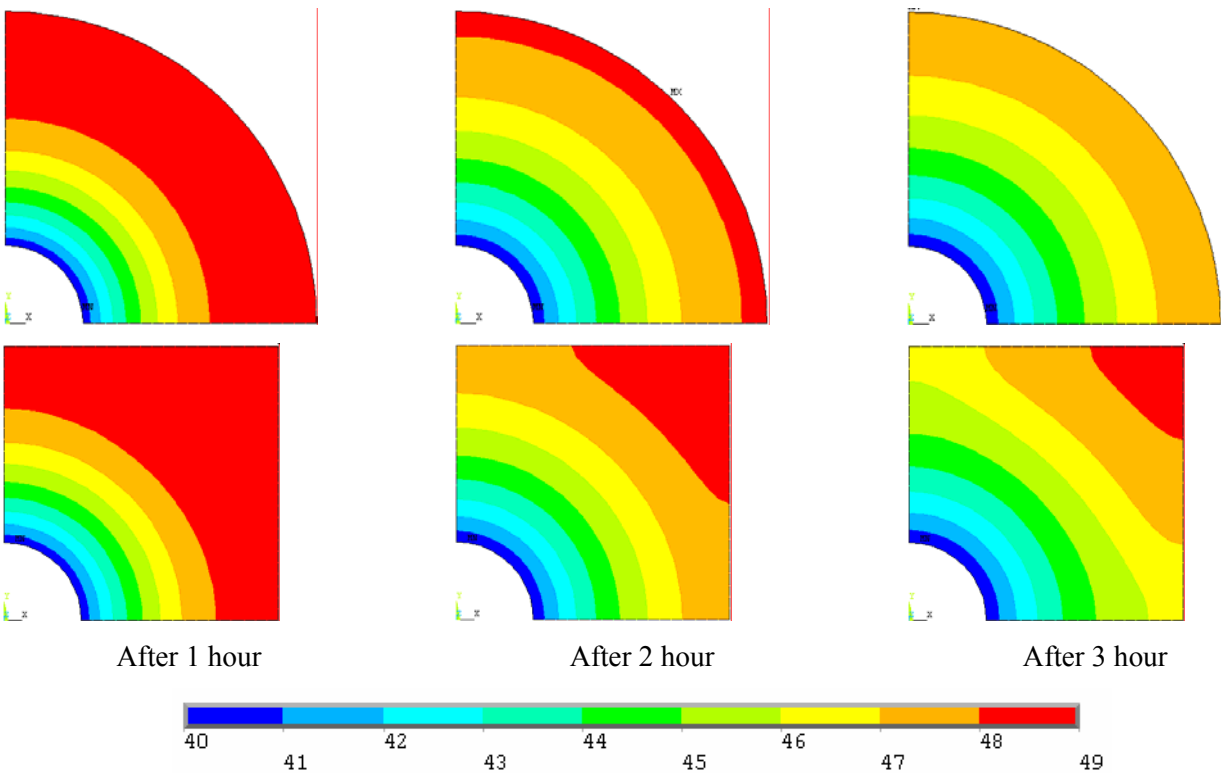
Figure 11 Temperature Distributions at Different Time during solidification Process.
PCM2/Vol.3; $\Delta T = 15$ ℃, $m_f = 1$ l/min.
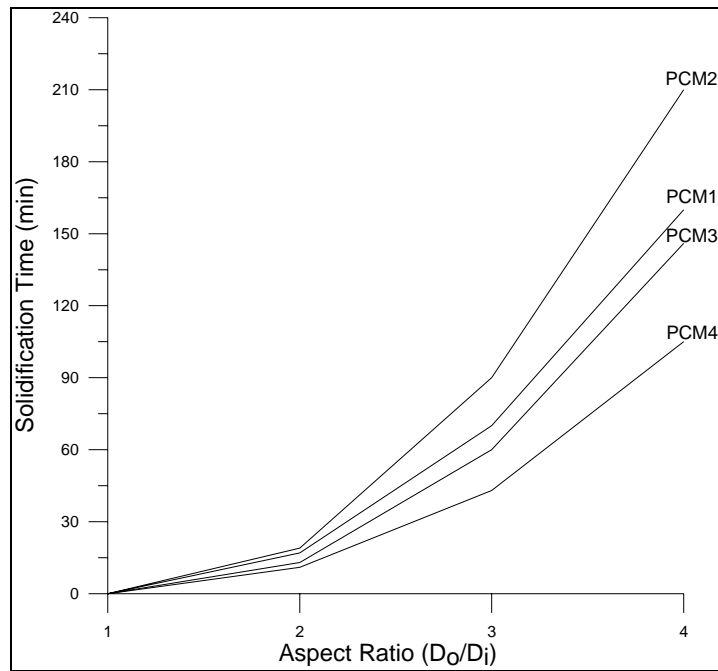
Figure 12 Effect of Aspect Ratio (container volume) on Solidification time for various PCM;
$\Delta T = 25\ ^oC,\ m_f = 3$ l/min.
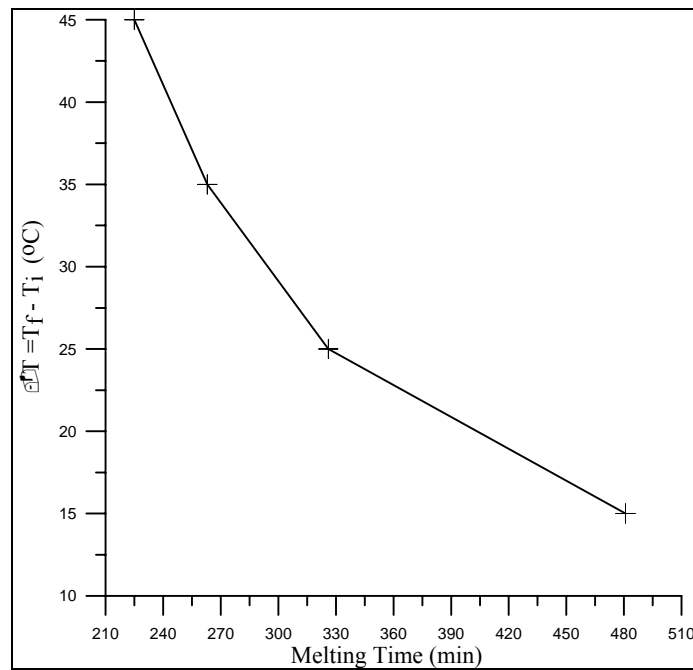
Figure 13 Effect of the Temperature Difference (ΔT) on the Melting Time of Paraffin (48 ^oC);
$m_f = 3$ l/min
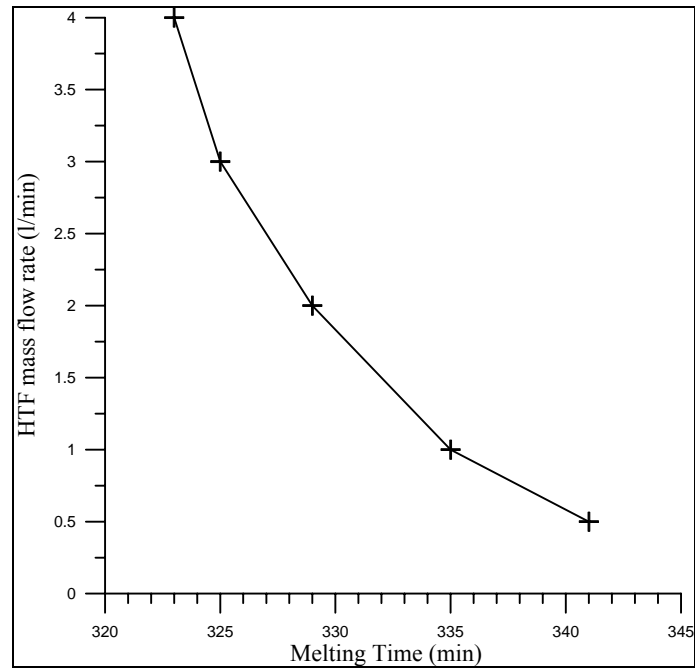
Figure 14 Effect of Different Mass flow rate of Heat Transfer Fluid (HTF) on the Melting Time of Paraffin (48 ^{o}C) ; $\Delta T = (T_f - T_i) = 25$ ^{o}C
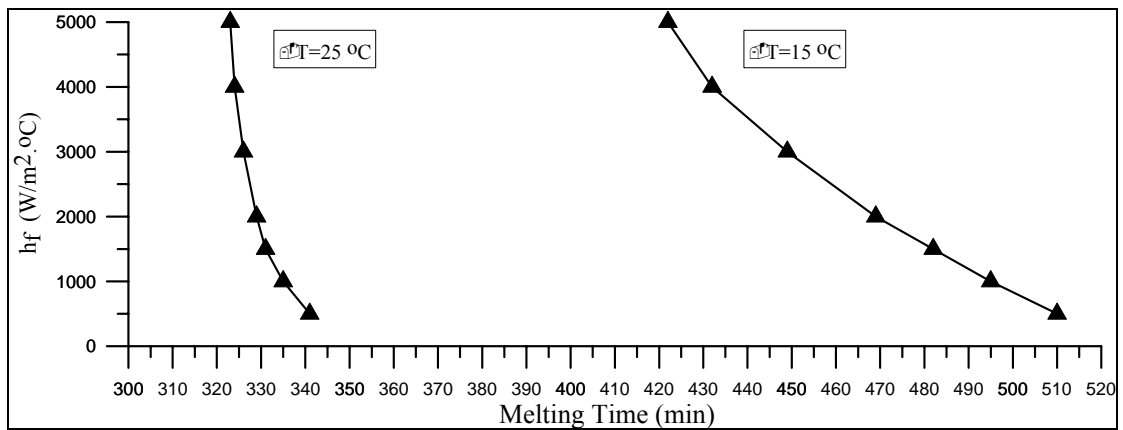
Figure 15 Effect of different convective heat transfer coefficient (h_f) on the melting time of Paraffin (48°C) at different Temperature difference
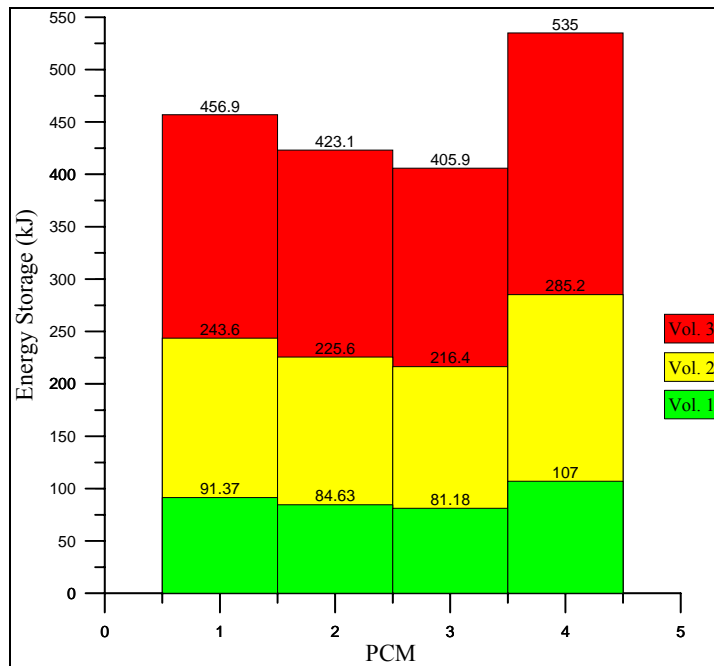
Figure 16 Energy Storage in various PCM at different container volume; $\Delta T = 25\ ^{o}C$
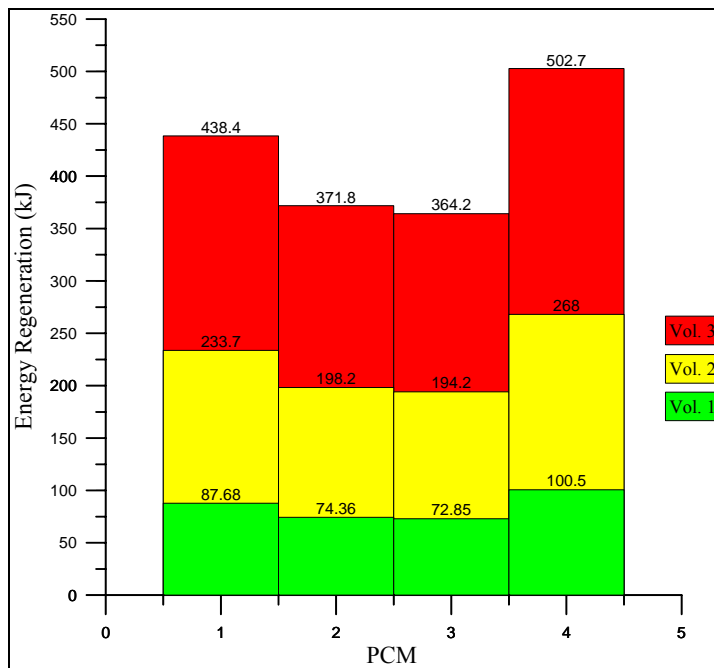
Figure 17 Energy Regeneration in various PCM at different container volume; $\Delta T = 25^{o}C$

NOMENCLATURE:

The symbols used in this paper have the following meanings:

Symbol	**Description**	**Units**
c_p	Specific heat	kJ/kg.K
D	Tube diameter	m, mm
h	Convection heat transfer coefficient	W/m^2.K
J	Jacobian	
k	Thermal conductivity	W/m.^{o}C
LH	Latent heat	kJ/kg
$\dot{m}$	Mass flow rate	kg/s, l/min
T	Temperature	^{o}C
t	Time	s, min
w	Side width	m, mm
x, y, z	Cartesian coordinates	m

Greek symbols

α'	Thermal diffusivity	m^2/s
$\alpha, \beta, \gamma, \lambda, \sigma$	Transformation coefficients	
ζ, η	Body-Fitted generalized Coordinates	
ρ	Density	kg/m^3
Δ	Difference	

Subscripts

av.	Average
eff.	Effective
b	Bulk
i	Initial, inner
i, j	Grid points
f	Final, fluid
l	Liquid
m	Melting
max.	Maximum value
o	Outer
s	Solid

Abbreviations

1,2D	One, Two-dimensions
asp.	Aspect Ratio
BFC	Body-Fitted Coordinate
HTF	Heat Transfer Fluid
LHTES	Latent Heat Thermal Energy Storage
PCM	Phase Change Material
RF	Relaxation Factor
SOR	Successive Over – Relaxation
vol.	Volume